



This is a repository copy of *Electrical/spectroscopic stability of conducting and biodegradable graft-copolymer*.

White Rose Research Online URL for this paper:

<https://eprints.whiterose.ac.uk/190247/>

Version: Published Version

---

**Article:**

Da Silva, A.C. [orcid.org/0000-0002-6258-9506](https://orcid.org/0000-0002-6258-9506), Paschoal, V.H., Ribeiro, M.C.C. et al. (1 more author) (2022) Electrical/spectroscopic stability of conducting and biodegradable graft-copolymer. *Macromolecular Chemistry and Physics*, 223 (19). 2200275. ISSN 1022-1352

<https://doi.org/10.1002/macp.202200275>

---

**Reuse**

This article is distributed under the terms of the Creative Commons Attribution (CC BY) licence. This licence allows you to distribute, remix, tweak, and build upon the work, even commercially, as long as you credit the authors for the original work. More information and the full terms of the licence here:

<https://creativecommons.org/licenses/>

**Takedown**

If you consider content in White Rose Research Online to be in breach of UK law, please notify us by emailing [eprints@whiterose.ac.uk](mailto:eprints@whiterose.ac.uk) including the URL of the record and the reason for the withdrawal request.



[eprints@whiterose.ac.uk](mailto:eprints@whiterose.ac.uk)  
<https://eprints.whiterose.ac.uk/>

# Electrical/Spectroscopic Stability of Conducting and Biodegradable Graft-Copolymer

Aruã Clayton Da Silva,\* Vitor Hugo Paschoal, Mauro Carlos Costa Ribeiro, and Susana Inés Córdoba de Torresi\*

Development of conductive and biodegradable graft-copolymers is decisive for applied electrical biointerfaces. However, to make significant breakthrough in bioelectronics, addressing changing properties while degrading is essential. Herein, the conductive and biodegradable poly(3,4-ethylenedioxythiophene) and poly(D,L-lactic acid) copolymer (PEDOT-co-PDLLA) submitted to 35 days of degradation in either deionized water or phosphate-buffered saline (PBS) is reported. Cyclic voltammetry, electrochemical impedance spectroscopy, and Raman microspectroscopy are used to correlate the electrical stability with molecular/structural changes during the degradation process. Two different proportions 1:05 (higher PEDOT content) and 1:50 (lower PEDOT content) are evaluated. The PEDOT-co-PDLLA 1:05 presents stable charge storage capacitance (CSC) in PBS for 35 days. PEDOT-co-PDLLA 1:50 shows an enhanced CSC when freshly prepared. However, it promptly loses its capacitance. Raman spectroscopy demonstrates that 1:05 as-prepared shows mostly neutral state. Nonetheless, after 35 days of degradation, both graft-copolymers show similar spectra, with contributions of oxidized states. Although the increase in oxidized states moieties should improve the conductivity, its dependence on interconnectivity and its relevance to remaining electronically stable, intrinsically related to conductive/biodegradable proportions in as-prepared graft-copolymer are demonstrated. This work contributes to a better understanding of the electrical stability of graft-copolymers for designing smart devices in bioelectronics applications.


## 1. Introduction

Electrically conductive biomaterials with suitable physical/biological properties of tissues are highly desired for bioelectronics technologies.<sup>[1–4]</sup> In this context, conducting polymers (CPs) appear with a great potential for designing a whole new generation of soft biointerfaces.<sup>[5,6]</sup> The idea of applying CPs as biomaterial by strategically linking conductive to biodegradable blocks that offer momentaneous electrical property is fascinating. After their use, these materials completely disappear (via macrophages) without significant damage to the organism, showing tremendous potential in the biomedical field.<sup>[7,8]</sup> Later, novel biomaterials based on block-copolymers, mainly based on polyaniline (PANI), have rapidly risen.<sup>[9–20]</sup> Many successful approaches to obtaining such a conductive and biodegradable block-copolymer were achieved. However, the conductivity of PANI is intrinsically related to its acidity or doping with acid molecules,<sup>[21–23]</sup> a challenging condition when working under physiological conditions, which results in its electrical behavior being compromised, limiting its applications. In addition, issues with biocompatibility have been explored as antimicrobial, antibacterial, and antioxidant activity.<sup>[24–32]</sup> As an alternative to

A. C. Da Silva, S. I. C. de Torresi  
 Laboratório de Materiais Eletroativos, Departamento de Química Fundamental  
 Instituto de Química  
 Universidade de São Paulo  
 Avenida Prof. Lineu Prestes, 748, São Paulo, Butantã 05508-900, Brazil  
 E-mail: a.dasilva@sheffield.ac.uk; storresi@iq.usp.br

A. C. Da Silva  
 Implantable Bioelectronics Laboratory  
 Department of Automatic Control and Systems Engineering  
 Faculty of Engineering  
 University of Sheffield  
 Mappin Street, Sheffield, South Yorkshire S10 2TN, UK  
 A. C. Da Silva  
 Insigneo Institute for in silico Medicine  
 University of Sheffield  
 The Pam Liversidge Building, Sheffield S10 2TN, UK

V. H. Paschoal, M. C. C. Ribeiro  
 Laboratório de Espectroscopia Molecular, Departamento de Química Fundamental, Instituto de Química  
 Universidade de São Paulo  
 Avenida Prof. Lineu Prestes, 748, São Paulo, Butantã 05508-900, Brazil

 The ORCID identification number(s) for the author(s) of this article can be found under <https://doi.org/10.1002/macp.202200275>

© 2022 The Authors. Macromolecular Chemistry and Physics published by Wiley-VCH GmbH. This is an open access article under the terms of the Creative Commons Attribution License, which permits use, distribution and reproduction in any medium, provided the original work is properly cited.

DOI: 10.1002/macp.202200275

enhance biocompatibility, several materials appear with great potential for application, such as poly(3,4-ethylenedioxythiophene) (PEDOT)<sup>[33–38]</sup> and inert carbonaceous materials in composites (e.g., carbon nanotubes and graphene).<sup>[39–41]</sup>

Although the development of conductive and biodegradable graft-copolymers is not entirely new, it has recently been hugely increasing.<sup>[42–47]</sup> However, novel graft-copolymers studies are typically focused on physical–chemical characterization instead of advancing on biomedical applications.<sup>[48–57]</sup> A critical factor in advancing its applications in biomedical or even point-of-care applications is to understand its stability and the degradation mechanisms since graft-copolymers are usually referred to as erodible or bioerodible, i.e., they become soluble in physiological media through the biological action, given that the conductive moiety is not degradable by itself. Thus, it often remains the pure CPs, limiting applications for implantable bioelectronics. In 2011, Jang and colleagues investigated cellular uptake and cytotoxicity of CP nanospheres ( $\approx 22$  nm) toward mouse macrophage RAW 264.7 and rat pheochromocytoma PC-12 cells and found that all were internalized via phagocytosis and endocytosis.<sup>[58]</sup>

In previous work, we demonstrated the design of a conducting and “partially” biodegradable graft-copolymer based on PEDOT-co-PDLLA (poly(D,L-lactic acid)). Different strategies for modification of macromonomer (EDOT-PDLLA), achieving different conductivities and biodegradability (hydrolytically) were proposed.<sup>[59]</sup> Afterward, it was also demonstrated that materials with different proportions from EDOT to EDOT-PDLLA were conductive, biodegradable (enzymatically), and showed good biocompatibility for embryonic stem cells with great potential induce neuronal differentiation.<sup>[60]</sup> The synthetic approach uses an organic media with inorganic oxidant salt (ammonium persulfate) in suspension, resulting in an organic fraction containing soluble PEDOT-PDLLA and an insoluble pure PEDOT which is discarded. Characterization of these materials suggested that the PEDOT oligomers were obtained and that, therefore, they could be easily eliminated from the body via macrophages.<sup>[58,61]</sup> Recently, Mecerreyes and colleagues have demonstrated an optimization for 3D printing by direct ink writing the PEDOT-poly(lactic acid) and PEDOT-poly  $\epsilon$ -caprolactone graft-copolymer.<sup>[62,63]</sup>

The electrical stability of PEDOT polymers was investigated mainly using the commercially available suspensions of PEDOT and poly(styrenesulfonate) (PEDOT:PSS).<sup>[37,64,65]</sup> In addition, additives such as surfactants, acid treatment, ionic liquids, or organic molecules were also demonstrated to enhance the electrical properties of PEDOT.<sup>[66–69]</sup> On the one hand, such approaches can work quite well outside bioelectronics applications (i.e., solar cells devices or organic transistors), on the other hand, they could hardly be translated due to the lack of biocompatibility. Focusing on the electrical stability for bioelectronics, Green and colleagues investigated the adhesion to substrates and conductivity for different dopants of PEDOT over Pt electrodes.<sup>[70]</sup> Moreover, Mawad and colleagues demonstrated the electrical stability of PANI in phosphate-buffered saline (PBS) for 14 days, aiming for cardiac models.<sup>[71]</sup>

The development of novel methodologies to accurately determine the electrical stability of conductive graft-copolymer is still desired. Here, we report the electrical/spectroscopic stability of the graft-copolymer while degrading by using electrochemical

techniques and Raman spectroscopy mapping. In addition, two different proportions of PEDOT to PDLLA were investigated. Combining electrical and vibrational information makes it possible to access the structural changes and correlate them with the electroactivity of the PEDOT while degrading.

## 2. Results

### 2.1. Degradation Essay

The degradation tests of the graft-copolymers were already reported following standardized protocols for biomaterials in the presence and absence of enzymes.<sup>[59,60]</sup> However, herein a distinct degradation experiment was designed to avoid adding exogenous chemicals (e.g., buffers or antibiotics) to characterize the remaining graft-copolymer film with minimal modifications.

Figure 1 shows pictures representing the physical aspects of the PEDOT-co-PDLLA films before (Figure 1a) and after (Figure 1b) 35 days of degradation by the weight loss method. The PEDOT-co-PDLLA films in the proportions of 1:05 and 1:50 presented  $60.4 \pm 13.1\%$  and  $91.4 \pm 0.8\%$  weight loss after 35 days of degradation in deionized water, respectively. In a previous study, the hydrolytic degradation (in PBS) resulted in  $\approx 20\%$  and  $80\%$  weight loss after 35 and 120 days, respectively.<sup>[59]</sup> Thus, it is possible to identify the difference between a buffered and unbuffered medium since, in the latter condition, the acidity can build up and promote faster hydrolysis. It is noteworthy that, in the presence of the PBS, the pH does not decrease beyond 7.2 for the most degraded conditions (Supporting Information Figure S1). Additionally, the enzymatic degradation (using Proteinase K) resulted in 29–46% weight loss after 35 days.<sup>[60]</sup> The highlight of Figure 1a represents the graft-copolymer film at the initial state (left), where it is possible to see a somewhat homogenous film of the copolymer, which was obtained over a glass substrate with the as-prepared chemical structure of the graft-copolymer shown in the left panel of Figure 1c. In the degraded stage (highlighted in Figure 1b), the remaining mass is mainly composed of insoluble grains of degraded PEDOT moieties. The PDLLA moiety is hydrolyzed by water, and its oligomers go to the aqueous solution, with its chemical structure shown in the right panel of Figure 1c. The same experiments were done in parallel over a glassy carbon electrode (GCE) for electrochemical measurements (Figure 1d). We used PBS (pH = 7.4) as a degradation medium and supporting electrolyte for the electrochemical experiments to mimic an environment without much pH change, like physiological conditions. It is critically important to avoid a rash acidic condition once acid treatment is well known to enhance PEDOT electronic property.<sup>[72]</sup> Therefore, we have added a counter electrode (platinum coil) and reference (Ag/AgCl/KCl saturated) and promoted electrochemical experiments while the graft-copolymer was degrading (Figure 1d). Afterward, the GCE was removed from the degrading solution and submitted to Raman spectroscopy shortly after the electrochemical experiments (Figure 1e).

The remaining solid from the degradation process of the graft-copolymer PEDOT-co-PDLLA is not characterizable by traditional methods (e.g., gel permeation chromatography (GPC) or matrix-assisted laser desorption ionization-time-of-flight mass spectrometry) due to its insolubility in most common solvents. Therefore, we have analyzed the soluble portion by high-performance

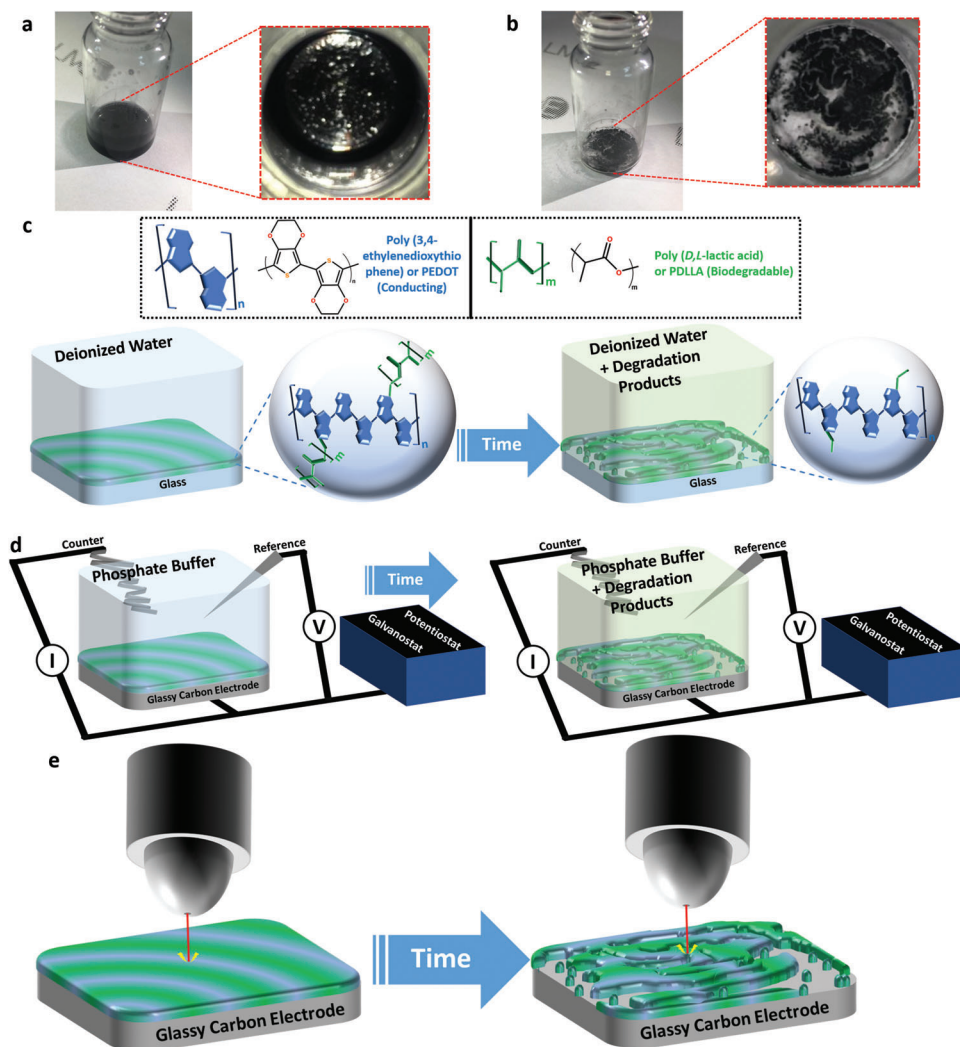


**Figure 1.** Degradation assay and characterization methods. a) Photographs of the PEDOT-co-PDLLA films before degradation and b) after 35 days of degradation essay. c) Schematic representation with structural changes in graft-copolymer in the process of degradation, produced over glass vials in deionized water. In parallel, thin PEDOT-co-PDLLA films were produced over glassy carbon electrodes (GCE) and incubated in PBS (pH = 7.4). d) The graft-copolymer produced over GCE was connected to potentiostat/galvanostat and electrochemical characterizations were investigated. e) At the same time, the PEDOT-co-PDLLA films were removed from degradation solution and submitted to Raman spectroscopic characterization. More samples were prepared over ITO-covered glass and submitted to Raman microscopy mapping before and after 35 days of degradation essay.

liquid chromatography mass spectrometry (HPLC-MS) and  $^1\text{H}$  NMR (Supporting Information Figures S2 and S3). We identified that the degraded PDLLA composition is poly (D, L-lactic acid) oligomers with  $\text{pH} \approx 4.0$ , as already demonstrated.<sup>[73–75]</sup> Additionally, the soluble extracts were cultivated with keratinocytes (HaCaT) cells for 24 h (Supporting Information Figure S4). We have observed that up to 10% v/v dilution, this extract remains biocompatible (superior to 70% viability), and its lethal dose (LD50) is superior to 15% v/v. The remaining solid of the graft-copolymer films deposited on indium-tin oxide-covered glass (ITO) were characterized by Raman spectroscopy (which will be discussed further ahead) and UV-vis absorption spectroscopy with the results shown in Supporting Information Figure S5. The UV-vis spectra present absorptions through the whole spectrum, especially at low wavelengths. This absorption likely is associated with its dark color (dark blue/black), and it is noteworthy that

the higher the PEDOT content, the darker the color aspect of the film.

## 2.2. Electrochemical Stability

The electrical performance of conductive biomaterial is very dependent on several parameters such as media (electrolyte) and previous treatments (e.g., temperature, solvents, or pH), among others. **Figure 2a** shows atomic force microscopy (AFM) images of PEDOT-co-PDLLA films i) 1:05 and ii) 1:50, evidencing its surface roughness. From surface analysis, we obtained for  $50 \times 50 \mu\text{m}^2$  and  $10 \times 10 \mu\text{m}^2$  images the root-mean-square average of height deviation ( $R_q$ ) and the arithmetic average of the absolute values of height deviations ( $R_a$ ) (Supporting Information Table T1). It can be observed that both surfaces present

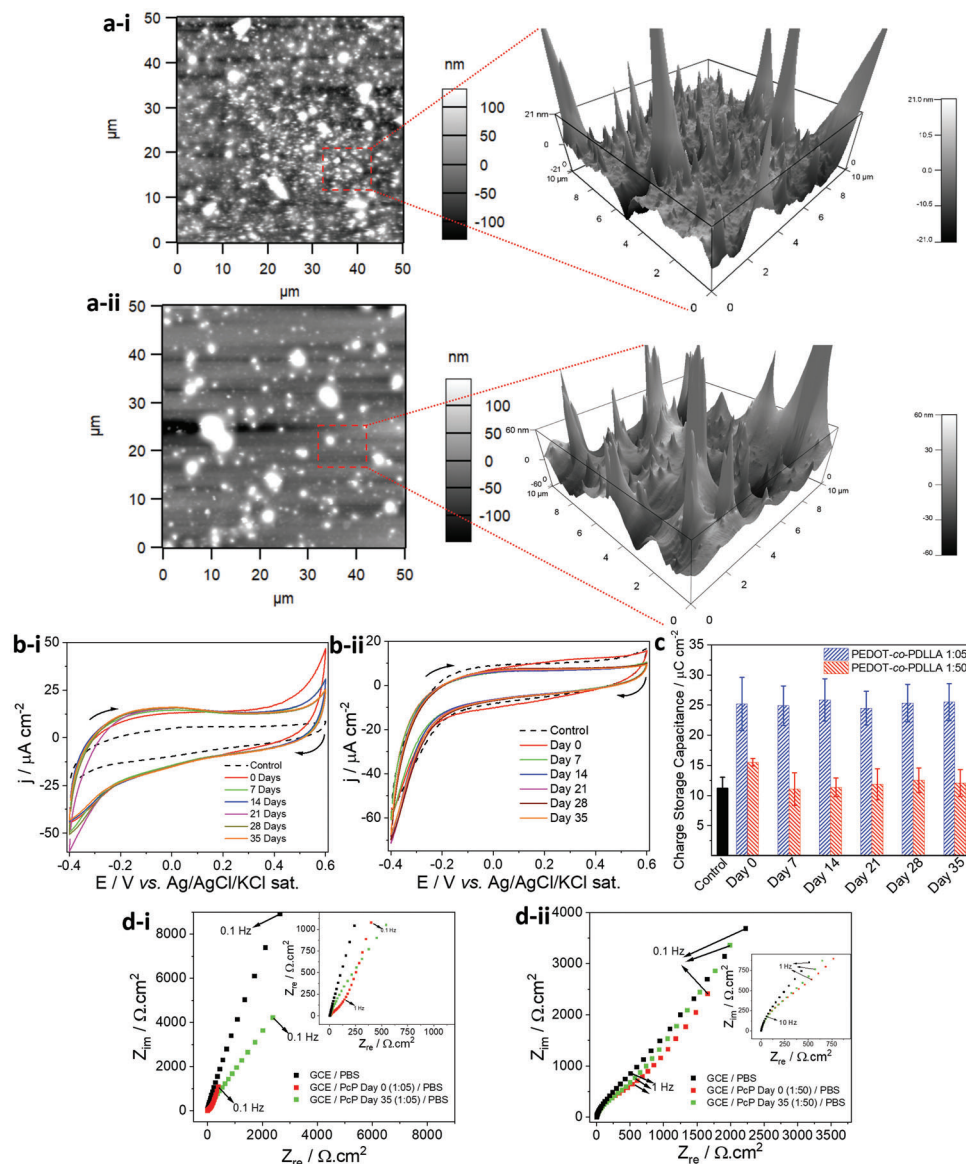


**Figure 2.** Physical and electrochemical characterizations. a) Atomic force microscopy (AFM) images  $50 \times 50 \mu\text{m}^2$  of the PEDOT-co-PDLLA films i) 1:05 and ii) 1:50 with amplification for  $10 \times 10 \mu\text{m}^2$  3D AFM images. b) 10th CV scan of PEDOT-co-PDLLA i) 1:05 and ii) 1:50 while degrading with bare GCE (black, dotted) in PBS solution ( $\text{pH} = 7.4$ ), respectively. c) CSC for each interface while degrading, calculated from CV. d) Nyquist plot of PEDOT-co-PDLLA i) 1:05 and ii) 1:50 thin films freshly prepared (red) and after 35 days of degradation (green) with bare GCE as control (black) recorded in PBS ( $\text{pH} = 7.4$ ) at OCP condition, respectively.

similar roughness for the larger sampled areas ( $50 \times 50 \mu\text{m}^2$ ). However, for the smaller areas ( $10 \times 10 \mu\text{m}^2$ ), the PEDOT-co-PDLLA 1:05 is rougher than 1:50, with more grains over the surface. Likely, 1:05 is more conductive and has more well-doped grains.<sup>[76]</sup> The intrinsic conductivity of the PEDOT-co-PDLLA 1:05 and 1:50 graft-copolymers were  $5.35 \times 10^{-5}$  and  $4.19 \times 10^{-8} \text{ S cm}^{-1}$ , respectively.<sup>[60]</sup> Figure 2b-i,ii shows the 10th cycle of cyclic voltammetry (CV) scan of PEDOT-co-PDLLA 1:05 and 1:50 films in PBS. The PEDOT-co-PDLLA 1:05 presents a capacitive behavior, clearly superior to the GCE control surface, slightly increasing while degrading. The slight increase in capacitance suggests the PEDOT is getting more doped while de-

grading. The PEDOT-co-PDLLA 1:50 also presents a capacitive behavior. However, its capacitance is superior only when freshly prepared. After 7 days, the current is lower than the GCE control surface. Figure 2c shows the CSC calculated from the 10th cycle of CV in PBS. The PEDOT-co-PDLLA 1:05 is electrically stable during 35 days of degradation in PBS solution, while 1:50 only presents significantly higher CSC when freshly prepared. The graft-copolymer of PEDOT-co-PDLLA 1:05 (higher PEDOT content) presents a long-term electrical stability in PBS for 35 days. The rapid decrease in the CSC for the PEDOT-co-PDLLA 1:50 is likely due to the faster degradation and loss of the interconnectivity.

Before performing the electrochemical impedance spectroscopy (EIS) experiments, the interfaces' open circuit potential (OCP) was measured for at least 30 min (Supporting Information Table T2). We observed that the OCP before and after 35 days of degradation increased by +80 mV for PEDOT-*co*-PDLLA 1:05. However, the OCP did not significantly change for the 1:50 copolymer. Additionally, the OCP after degradation does not reach the value of the bare GCE surface. It suggests that the PEDOT remaining over the surface still affects OCP and the electrical behavior of the interface. Supporting Information Figure S6 shows CVs of PEDOT-*co*-PDLLA with highlighted points of OCP and +0.4 potential where EIS was carried out.

The Nyquist plot for the PEDOT-*co*-PDLLA graft-copolymers in PBS for i) 1:05 and ii) 1:50, respectively, are evidenced in Figure 2d. Figure 2d-i shows that the capacitance component (at low frequency, 0.1 Hz) when freshly prepared (green) is lower than the GCE interface. Also, the capacitance component significantly increases after 35 degradation days (red). Finally, the resistance component (inset) increases after the degradation period. It suggests that the PEDOT structure is doped with the degradation process, agreeing with CV (Figure 2b-i). Figure 2d-ii shows that the PEDOT-*co*-PDLLA 1:50 slightly increases the capacitance and decreases resistance (inset). The Bode plot demonstrated that for 1:05, the total impedance decreases from 295 to 154 and 37 k $\Omega$  cm<sup>2</sup> at 0.1 Hz when compared to control. While for 1:50, the total impedance slightly decreases from 137 to 124 and 93 k $\Omega$  cm<sup>2</sup> in the low-frequency region (Supporting Information Figure S7). The decrease in total impedance means the interface is more conductive than the control. It suggests the remaining PEDOT still improves the conductivity of the GCE electrode, even after the degradation. An EIS measurement at a different potential than the OCP (in this case +0.4 V) was also tested and is shown in Supporting Information Figure S8. The +0.4 V was chosen because it is inside the electrochemical window of PEDOT, where it shows a capacitive behavior (Supporting Information Figure S5). The results at +0.4 V are similar to the above discussed, agreeing with the OCP measurement.

It was not possible to obtain an equivalent electrochemical circuit using the EIS spectra in PBS. Thus, CV and EIS experiments were also carried out in the presence of the redox couple [Fe(CN)<sub>6</sub>]<sup>4-</sup>/[Fe(CN)<sub>6</sub>]<sup>3-</sup> as an electrochemical probe (Figure 3). Figure 3a-i shows the CV voltammogram of the control, pristine (day 0), and degraded (day 35) PEDOT-*co*-PDLLA 1:05. The day 0 sample presents a lower current and slightly higher peak separation (160 mV), while the 35-day sample reaches a higher current and lower peak separation (88 mV). Likely, the remaining PEDOT is still electroactive and well-doped after degradation time. Figure 3a-ii shows that the 1:50 graft-copolymer presents similar performance: lower current and higher peak separation (144 mV) at day 0, but higher current and lower peak separation (110 mV) after 35 days of degradation.

Figure 3b-i,ii shows the Nyquist plot for the graft-copolymers before and after degradation. Both present similar resistance to the GCE control surface (black and red) at day 0. However, the resistance significantly increases after the degradation (green). We further analyzed these data using the redox probe and fitted it with the Randles circuit (Figure 3c), for which the  $\chi^2$  values were very close to zero ( $\approx 0.0030$ ), which strongly suggests an excellent data fitting to the equivalent electrochemical circuit model. The

Warburg coefficient was omitted since it is related to the diffusion coefficient of the redox probe. Figure 3d shows a table summarizing the relevant parameters obtained from EIS experiments with the electrochemical probe.

The value of  $R_s$  (solution resistance) did not significantly change between measurements once the PBS was renewed for every measurement. However,  $R_{CT}$  (charge-transfer resistance) significantly increased 2.5 times with degradation time for both graft-copolymers. Additionally, it is possible to see that  $\alpha$  (deviation from ideal capacitive behavior) is slightly lower for the 1:50 sample, likely because it is more resistive than 1:05 (i.e., less conductive). In either case, the  $\alpha$  values being close to 1 evidence that both graft-copolymers have significant capacitive behavior, in agreement with previous observations. The capacitance of PEDOT-*co*-PDLLA 1:05 and 1:50 decreased by 33% and 36% with the degradation process, respectively. After 35 days of degradation of 1:05 graft-copolymer, the resulting higher capacitance agrees with CSC values obtained in PBS (Figure 2c).

### 2.3. Spectroscopic Stability

For CPs, Raman spectroscopy is a powerful tool to access structural changes only in the conductive component once typically, CPs have larger cross-sections or could even have their intensity enhanced by the Raman resonance effect.<sup>[77–79]</sup> This point is further illustrated by comparing the calculated nonresonant cross-sections of a two and four-unit EDOT oligomer to a three-unit PDLLA oligomer, shown in Supporting Information Figure S9. Thus, we will focus on the spectroscopic changes occurring on PEDOT in this work.

Figure 4a evidences a schematic representation of the Raman microscope mapping through the PEDOT-*co*-PDLLA graft-copolymer films. Here, we prepared samples either over GCE (same samples of the electrochemical experiments) or ITO-covered glass (specifically prepared for Raman microspectroscopy). Figure 4b shows an optical image of the PEDOT-*co*-PDLLA 1:05 film overlaid with chemical mapping of the most intense band at 1433 cm<sup>-1</sup>. The Raman spectra of the PEDOT-*co*-PDLLA films deposited over GCE (GCE/PEDOT-*co*-PDLLA) in pristine (as-synthesized, top) and degraded (for 35 days, bottom) are shown in Figure 4c. From our calculations, in agreement with previous results from the literature, it is promptly observed that the pristine PEDOT only show very few Raman active modes (blue line) with very high cross-sections in the range of 1400–1600 cm<sup>-1</sup> and others with low cross-sections in the range of 200–1400 cm<sup>-1</sup>.<sup>[80]</sup> Other features, precisely down to 500 cm<sup>-1</sup>, may be related to the presence of the oxidized species (polaronic or bipolaronic, red and purple lines).

Figure 4d shows the normal modes' displacement vectors with the highest cross-sections for the i) pristine and ii and iii) oxidized PEDOT chains. As observed in the case of oxidized chains, both modes are related to deformations along the bonded thiophene rings in the oligomer's plane and the hydrogen atoms out of this plane. Regardless of the sample, an overall trend can be observed concerning sample degradation: the most intense bands become sharper and shift to a similar wavenumber ( $\approx 1429$  cm<sup>-1</sup>). Mainly, this frequency shift is very sensible for the 1:05 sample (less than

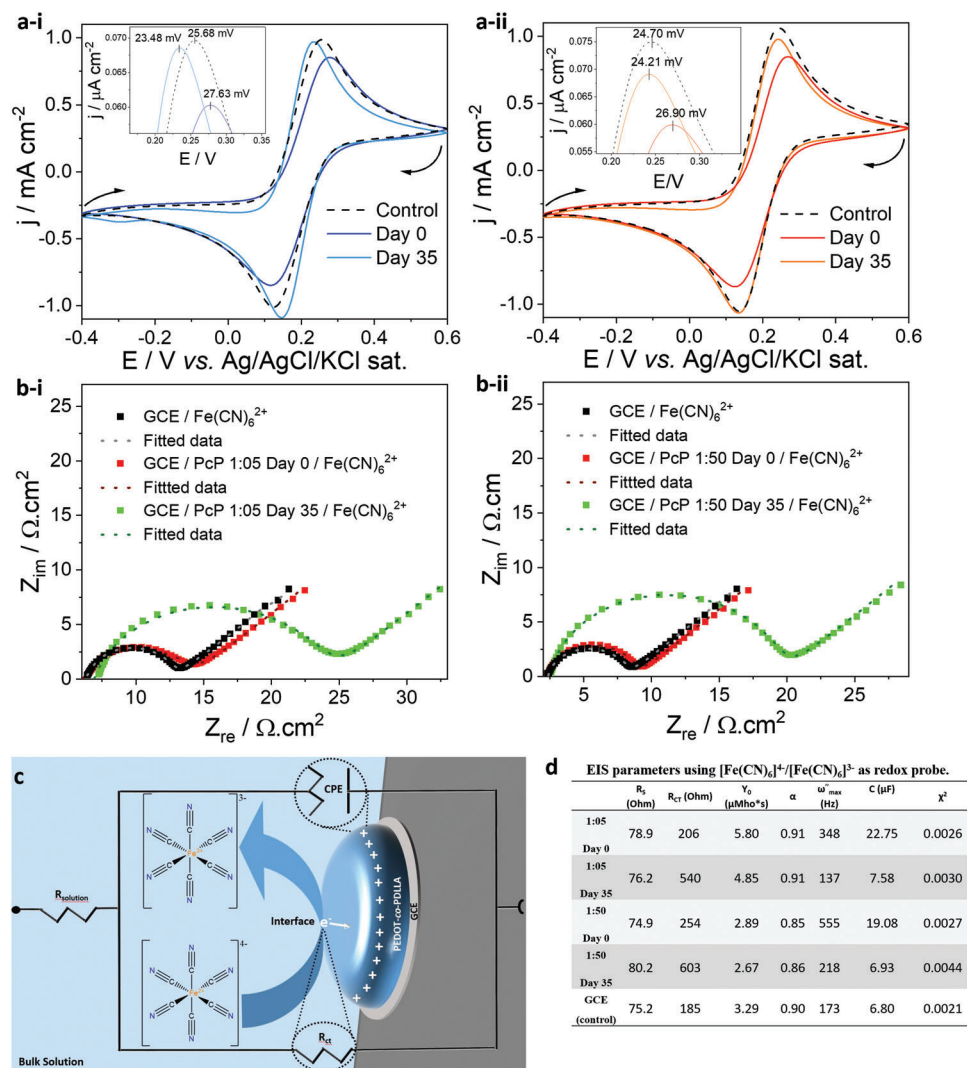


**Figure 3.** Electrochemical characterization with redox probe. a) 10th CV scan in  $[\text{Fe}(\text{CN})_6]^{4-}/[\text{Fe}(\text{CN})_6]^{3-}$   $10 \times 10^{-3}$  M solution for PEDOT-co-PDLLA i) 1:05 and ii) 1:50. Inset for highlighted oxidation peak shifts electric potentials. b) Nyquist plot of films freshly prepared (red) and after 35 days of degradation (green) with bare GCE (black), data (scatter/line), and fitted data (dotted line in dark color) recorded in  $[\text{Fe}(\text{CN})_6]^{4-}/[\text{Fe}(\text{CN})_6]^{3-}$   $10 \times 10^{-3}$  M solution for PEDOT-co-PDLLA i) 1:05 and ii) 1:50, respectively. c) Representation scheme of fitted circuit model which describes the graft-copolymer interface in the presence of  $[\text{Fe}(\text{CN})_6]^{4-}/[\text{Fe}(\text{CN})_6]^{3-}$ . d) EIS parameters using  $[\text{Fe}(\text{CN})_6]^{4-}/[\text{Fe}(\text{CN})_6]^{3-}$  as redox probe, where  $R_s$  represents the resistance of solution,  $R_{CT}$  is the resistance in charge-transfer of the iron complex, CPE is the constant phase element (for inhomogeneous or imperfect capacitance),  $\gamma_0$  is the admittance,  $\alpha$  is the deviation from ideal capacitive behavior,  $\omega_{max}$  is the frequency where the imaginary component is higher, and C is the capacitance of the hydrogel. The fitted models also have a Warburg coefficient in series with  $R_{CT}$ , but it is not represented because it is related to diffusion coefficient of iron complex ions.

$2 \text{ cm}^{-1}$ ) and much more prominent in the case of the 1:50 sample ( $\approx 5 \text{ cm}^{-1}$ ).

Based on our quantum chemical calculations for  $[\text{EDOT}]_{12}^{n+}$  ( $n = 0, 4$  or  $12$ , Figure 4c), we can infer that every sample has a different ratio between neutral and polaronic oligomers. Additionally, only small amounts of bipolaronic (overoxidized species) are present since its high Raman cross-section (even larger than that of neutral  $[\text{EDOT}]_{12}$ ) would allow their detection very easily. Thus, these results suggest the doping of the copolymers with degradation, associated with the frequency shift of the most intense band to lower frequencies. This behavior corresponds to an average trend of these samples over the GCE electrode, which

provides a coarse view of these systems. We can further explore these trends for PEDOT-co-PDLLA graft-copolymers using Raman microscopy and chemometrics.

Specifically, PCA (principal component analysis) was applied to analyze the Raman microspectroscopy results. Figure 4e shows the principal components of PCA of the Raman mappings (each point corresponds to a single spectrum obtained during the mapping) of the pristine and degraded samples and their loadings. Both degraded samples (blue and red circles for 1:05 and 1:50, respectively) show similar clustering. The pristine 1:05 and 1:50 (shown as gray squares and circles, respectively) are dispersed around PC1, with the first in the direction of negative PC2 val-

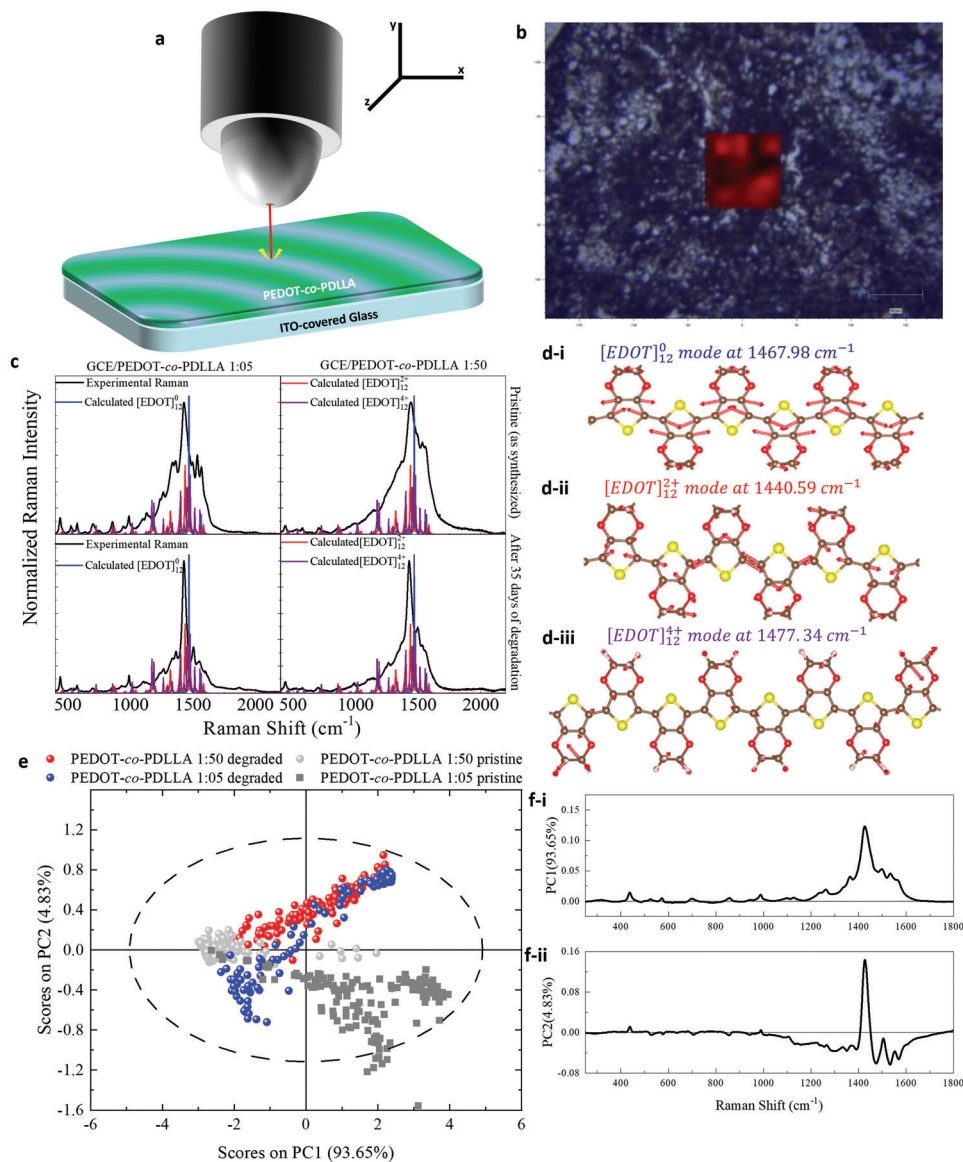


**Figure 4.** Raman spectroscopic characterizations. a) Schematic representation of the Raman microscope mapping through the graft-copolymer film over a conductive substrate (GCE or ITO). b) Optical image of PEDOT-co-PDLLA 1:05 pristine with chemical mapping obtained scanning the intense band  $1433 \text{ cm}^{-1}$ . c) Experimental Raman spectra of the GCE/PEDOT-co-PDLLA 1:05 (left) and 1:50 (right) pristine (top) and degraded (bottom). The calculated Raman cross-sections are shown in blue (neutral), red (oxidized), and purple (overoxidized). The curves are shown as Lorentzian band shapes of half-width at half-maximum of  $2 \text{ cm}^{-1}$  and the cross-section of the overoxidized species was divided by a factor of ten, all to improve visualization. d) Illustration of the normal mode displacement coordinates for the Raman active modes of the highest cross-section on six/eight middle units of a 12 unit long EDOT chain: i) neutral, ii) 2+ (or polaronic or oxidized), iii) 4+ (or bipolaronic or overoxidized). e) PC2 versus PC1 scores for the ITO/PEDOT-co-PDLLA samples: red and blue circles for the degraded 1:50 and 1:05 and gray circles and squares for the pristine samples. f) Loadings with experimental spectra for i) PC1 and ii) PC2.

ues and the latter spread around zero. The loadings for PC1 and PC2 are shown in Figure 4f-i,ii, with those related to PC1 resembling the spectra GCE/PEDOT-co-PDLLA 1:05, shown in Figure 4c. Thus, positive values for this PC1 are related to measurements across the ITO electrodes where PEDOT grains were measured. The clustering observed in Figure 4c makes it possible to identify that all degraded samples show more features related to oxidized PEDOT. Except for the pristine ITO/PEDOT-co-PDLLA 1:50 sample, only a few points are observed at positive PC1 val-

ues (likely due to a low proportion of PEDOT). The observation of a single (sharp) peak as in the PC2, on the other hand, resembles the spectra shown in Figure 4c (top-left) for the degraded sample of ratio 1:05. These results point to a scenario where the degraded samples are alike, showing more significant contributions of oxidized PEDOT species (mostly polaronic). Furthermore, the dispersion of the samples along PC1 and PC2 in contrast to their pristine counterparts (1:05 is mainly clustered at the fourth quadrant, and 1:50 is principally clustered around 0 for the



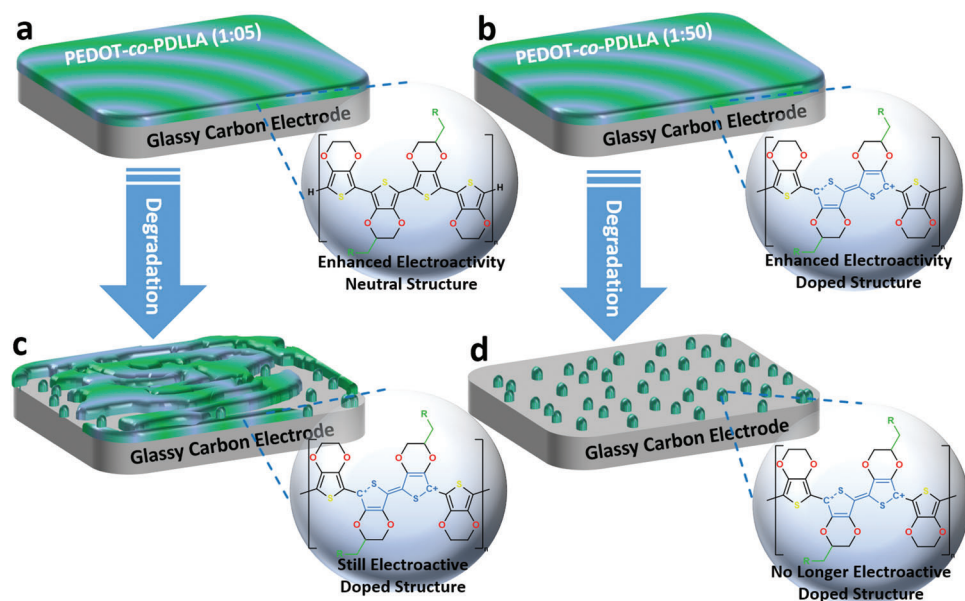


**Figure 5.** Electroactivity versus molecular aspects. a) Schematic representation of the PEDOT-*co*-PDLLA (1:05) graft-copolymer film as prepared with mostly neutral structure (benzoid) and enhanced electroactivity. b) Schematic representation of the PEDOT-*co*-PDLLA (1:50) graft-copolymer film as prepared with mostly doped structure (quinoid) and enhanced electroactivity. c) Schematic representation of the PEDOT-*co*-PDLLA (1:05) graft-copolymer film after the degradation period with mostly doped structure (quinoid) and still electroactive. d) Schematic representation of the PEDOT-*co*-PDLLA (1:50) graft-copolymer film after the degradation period with mostly doped structure (quinoid), but no longer electroactive.

PC2 axis) shows an increase in heterogeneity of the samples after degradation.

### 3. Discussion

There has been massive development in studies regarding the CPs and smart materials derived in the past decades. Initially, it resulted in many works seeking the highest conductivity possible, aiming for electronics applications. It positively impacted several areas, such as light-emitting diodes, field-effect transistors, and solar cells.<sup>[72]</sup> Unfortunately, the same strategy was applied in conductive biomaterials for biomedical and bioelectronics applications, which resulted in materials that lacked biocompatibility. Once the enhanced conductivity of CPs strategy requires treatment with typically hazardous chemicals (e.g., strong acids, ionic liquids, polar organic solvents, or surfactants), it indirectly creates an inverse relationship between conductivity and biocompatibility. The view of these two properties as adversarial led to experimental mistakes and misunderstandings in the biomedical and bioelectronics field. For instance, aniline-oligomers were first developed as block-copolymers for conducting and biodegradable copolymers.<sup>[14]</sup> Electrochemical characterizations were primarily performed using concentrated hydrochloric acid as an electrolyte and reported relatively high conductivity values.<sup>[81–83]</sup> Later, it was reported that the acidic doping in polyaniline negatively impacted cells.<sup>[84]</sup> It possibly resulted in this type of conductive biomaterials being explored for potential antibacterial properties.<sup>[85,86]</sup> In order to clarify some points in the interface between electronics and the bioelectronics/biomedical field, here we presented a protocol for investigating the electrical and spectroscopic stability with experiments designed to mimic physiological conditions.

Although the increasing amount of novel conductive biomaterials, the effects of conductivity/electroactivity when interfacing living cells are not entirely resolved. Our research group developed the PEDOT-*co*-PDLLA graft-copolymers and reported the conductivity of  $5.35 \times 10^{-5}$  and  $4.19 \times 10^{-8}$  S cm<sup>-1</sup> for 1:05 and 1:50, respectively.<sup>[60]</sup> Later, we investigated the effect of adhesion proteins over this biointerface. We found that the copolymer with lower conductivity had more homogeneously dispersed charges when the film was formed. It resulted in the adhesion of Fibronectin proteins in an unfolded conformation.<sup>[76]</sup> In another study, we quantified Fibronectin's adhesion and reported that fibroblasts' adhesion was significantly improved when electrically stimulated (+1 mV for 30 min).<sup>[87]</sup> Later, we demonstrated that capacitive electrical stimulation with an electrical field of 100 mV mm<sup>-1</sup> for 2 h day<sup>-1</sup> for 21 days significantly promoted osteogenic differentiation, remarkably better performance for higher PEDOT content.<sup>[88]</sup> Herein, we aimed to investigate the electrical stability of the graft-copolymers. **Figure 5** summarizes our findings, where the PEDOT-*co*-PDLLA 1:05 film remains connected and electroactive with better doping after the degradation period (Figure 5a,c). In the case of the 1:50 graft-copolymer, at a microscopic level, associated with thin-film integrity and homogeneity, we observe a significant loss of its interconnectivity rapidly. However, the PEDOT chains remain bound at a molecular level and are mainly in a doped state (Figure 5b,d). Advances toward the analysis of molecular-level analysis permitted an intriguing effect of electron transport (conformation-dependent) in single proteins (containing only simple amino acids without metallic center) to be reported.<sup>[89–91]</sup>

Recently, Bao and colleagues reported an engineered enzyme expressed in genetically targeted neurons able to synthesize conducting polymers (polyaniline and PEDOT) inside tissues of

living animals, evidencing that in low amounts, CPs can be biocompatible.<sup>[92]</sup> This marks an important achievement for the integration between living tissues and bioelectronics. Furthermore, it demonstrates the importance of advancing the studies of interactions at the conductive biointerfaces at the nanoscale and short-range for better bioelectronics system integration.

## 4. Conclusion

In the present work, we prepared conductive and biodegradable PEDOT-*co*-PDLLA graft-copolymer films in two different proportions (1:05 and 1:50), submitted them to degradation essays for 35 days and investigated their electrical and spectroscopic properties while degrading.

Using electrochemical methods, we found that the graft-copolymer with higher PEDOT content (1:05) presented higher capacitance and stability for the whole 35 days degradation period. However, the lower PEDOT content (1:50) presented increased capacitance only when freshly prepared, quickly losing it when degrading. Using spectroscopic methods, we found that the different materials became similar after the degradation process, with PEDOT in a more oxidized state (more doped), in agreement with electrochemical characterization for 1:05 graft-copolymer remained electroactive. However, although the 1:50 copolymer presents the doped structure, the remaining PEDOT is not enough to keep electroactive after 7 days of degradation. Likely due to the loss of interconnectivity while degrading.

## 5. Experimental Section

The synthesis method was developed in previous work.<sup>[59,60,93]</sup> Briefly, the first synthesis step was to obtain an electroactive macromonomer of EDOT-PDLLA. 3,6-Dimethyl-1,4-dioxane-2,5-dione (2.76 g, 20 mmol), hydroxymethyl EDOT (100 mg, 0.6 mmol), and tin (II)-2-ethylhexanoate (0.016 mL, 0.05 mmol) were stirred at 110 °C with 7 mL of toluene for 24 h. The solvent was removed by distillation under reduced pressure (20 mBar, 60 °C). The obtained solid product was purified by recrystallization with a (1:4) hexane/methanol mixture, separated by decantation and vacuum dried until constant mass. The yield obtained from this procedure was 98%. The EDOT-PDLLA was used as a chemical control because it was mainly formed by insulating PDLLA chains. <sup>1</sup>H NMR (500 MHz, CDCl<sub>3</sub>-*d*).  $\delta$  = 1.48–1.83 (m, 3H), 3.80–3.90 (m, 2H), 4.07–4.13 (m, 1H), 4.21–4.28 (m, 2H), 5.00–5.30 (m, 1H), 6.35 (s, 2H) ppm. <sup>13</sup>C NMR (500 MHz, CDCl<sub>3</sub>-*d*).  $\delta$  = 16.7, 66.7, 69.0, 69.2, 72.5, 116.4, 129.0, 169.4 ppm. GPC provided the  $M_n$  of 3.8 kDa,  $M_w$  of 5.5 kDa, and polydispersity index of 1.5.

The second step was consisted of obtaining the conducting and degradable copolymer of PEDOT-*co*-PDLLA. For this, 2.7 g of the macromonomer of EDOT-PDLLA was dissolved in 17.5 mL of dried acetonitrile and kept under magnetic stirring at 30 °C for 2 h. Subsequently, 3,4-ethylenedioxythiophene (EDOT) (0.06 g, 0.42 mmol) and NH<sub>4</sub>S<sub>2</sub>O<sub>8</sub> (0.18 g, 0.8 mmol) were added to the reaction vessel to obtain the molar proportion of 1:50 PEDOT:PDLLA, and kept under magnetic stirring at 30 °C for 24 h. After the reaction medium changed to dark blue, only the soluble fraction was placed in another glass vessel and the solvent was removed by distillation under reduced pressure (20 mBar, 60 °C), and the resultant solid was PEDOT-*co*-PDLLA. The feed molar proportion of PEDOT:PDLLA was 1:05 and 1:50, for which the actual molar proportion was 1:20 and 1:80 (determined by <sup>1</sup>H NMR), respectively. <sup>1</sup>H NMR (500 MHz, CDCl<sub>3</sub>-*d*).  $\delta$  = 1.48–1.83 (m, 3H), 3.80–3.90 (m, 2H), 4.07–4.13 (m, 1H), 4.20 (s, 2H, CH<sub>2</sub> of thiophenes), 4.21–4.28 (m, 2H), 5.00–5.30 (m, 1H), 6.32 (s, 2H) ppm. <sup>13</sup>C NMR (500 MHz, CDCl<sub>3</sub>-*d*).  $\delta$  = 16.7, 66.7, 69.0, 69.2, 72.5,

99.0 (C-thiophene), 116.4, 129.0, 169.4 ppm. GPC provided for PEDOT-*co*-PDLLA the  $M_n$  of 16.6 kDa,  $M_w$  of 18.6 kDa, and polydispersity index of 1.12.

The graft-copolymers of PEDOT-*co*-PDLLA in proportion of 1:05 or 1:50 films were immobilized onto substrates (glass vials, ITO glass, or GCE). Moreover, 20 mg mL<sup>-1</sup> solutions of each copolymer were prepared in chloroform; then, 200  $\mu$ L of each solution was slowly cast on the substrates (either GCE or ITO glass) by using an Ossila spin-coater under constant 3000 rpm rotation. For the degradation assay, 5 mL of copolymers solution was placed in a vial 2 cm in diameter and dried, resulting in at least 100 mg of weighted mass. Each vial with copolymer film was weighed and 5 mL of deionized water (Milli-Q) was added. The vials were placed in a 37 °C shaker at a rotating speed of 60 rpm. Copolymer films were withdrawn after 35 days and washed twice with deionized water. Films were dried in an oven at 50 °C overnight and vacuum-dried for 2 days to remove moisture. The experiments were performed in triplicate. Dry specimens were weighed, and the mass loss was calculated by Equation (1)

$$\text{Degradation (\%)} = \frac{W_0 - W_t}{W_0} \times 100 \quad (1)$$

where  $W_0$  is the initial mass of the copolymers film and  $W_t$  is the mass of copolymers film after time  $t$  (35 days).

HPLC coupled with MS was performed in CBM-20A (Shimadzu) coupled with Amazon Speed ETD (Bruker) equipped with an ESI source and a triple quadrupole mass spectrometer (Quatro Micro, Micromass). Mobile phase A: ultrapure water + 0.1% acetic acid. Mobile phase B: acetonitrile. Gradient: 0 to 60 min at constant 30% Eluent B. Column: Supelco Ascentis C-18 (250  $\times$  4.6 mm – 5  $\mu$ m). Flow: 1.0 mL min<sup>-1</sup>. Column temperature: 25 °C. Detection: for MS scanning in negative mode, argon was used as the drying (325 °C, 7 L min<sup>-1</sup>) and nebulizer of 27 Psi.

<sup>1</sup>H NMR spectra were recorded on a Bruker AIII 500 MHz spectrometer at 500 MHz. Chloroform-*d* (CDCl<sub>3</sub>) and deuterium oxide (D<sub>2</sub>O) were used as a solvent, and tetramethylsilane served as an internal standard.

Electrochemical experiments were performed using a multipotentiostat Autolab M101 (Metrohm), controlled by NOVA 1.11 software. All experiments were performed using four different GCE, a platinum sheet, and Ag/AgCl/KCl (saturated), as working, counter, and reference electrodes, respectively. For degradation, the electrodes with PEDOT-*co*-PDLLA films were stored in a closed chamber containing Dulbecco's PBS solution at room temperature. Before measurements, the electrodes were rinsed with water and placed in the electrochemical cell. CV experiments were performed in either PBS (pH = 7.4) or [Fe(CN)<sub>6</sub>]<sup>4-</sup>/[Fe(CN)<sub>6</sub>]<sup>3-</sup> 10  $\times$  10<sup>-3</sup> M solution at 10 mV s<sup>-1</sup> scan rate during 10 cycles every 7 days. CSC was calculated by integrating the current for the time of CV. EIS was measured over a 0.01 to 10<sup>5</sup> Hz frequency range and an amplitude of 10 mV at the OCP and 0.4 V. The OCP was measured at least 30 min before each measurement to reach the equilibrium of the interface. Double-layer capacitance was calculated by Equation (2)

$$C = Q (\omega''_{\max})^{1-\alpha} \quad (2)$$

where  $Q$  is a pseudocapacitance value,  $\alpha$  represents its deviation from ideal capacitive behavior,  $\omega''_{\max}$  represents the frequency at which the imaginary component reaches a maximum.<sup>[94–96]</sup>

Raman measurements of each sample (pristine and degraded) were obtained using a Renishaw inVia confocal microscope equipped with a 633 nm laser with maximum power at the output of 50 mW and 10 s long expositions. Two situations were considered during the spectroscopic characterization: in the first case, the thin films deposited over GCE (GCE/PEDOT-*co*-PDLLA) were considered as reference, to assess the samples' vibrational features. The second case was related to the samples deposited over an ITO substrate (ITO/PEDOT-*co*-PDLLA), which would more closely resemble the setup used for cell-growth experiments. The samples in the first case were measured using a long-working-distance 20x objective and 1% of the output laser power. The samples deposited over ITO substrates were mapped with long-working-distance of 20x and

50x, using 1% and 0.5% of the output laser power, respectively, to infer about the homogeneity of the films before and after degradation. For the mappings done with the 20x objective, three distinct regions of 320  $\mu\text{m}$  x 240  $\mu\text{m}$  were sampled along the ITO substrate. For the case of the 50x sample, a densely packed grid of points was sampled over a 90  $\mu\text{m}$  x 70  $\mu\text{m}$  area. The spectra of the mappings were processed using Matlab 9.2.0.538062 (R2017a) and the PLS Toolbox 8.8.1 (2020) by Eigenvector Research, Inc. Prior to the PCA all the mappings were analyzed simultaneously and were preprocessed using the Savitzky-Golay filter for smoothing (5-point window) and their baseline was corrected using alternating-least-square algorithm, and normalized by their maximum.

The analysis of the GCE/PEDOT-co-PDLLA samples was done with the support of quantum chemical calculations. Since the Raman cross-section of most PDLLA modes,<sup>[97]</sup> (as well as  $\text{SO}_4^{2-}$  counter ions) was very small when compared to those of PEDOT (as shown in Supporting Information Figure S9), only the former was considered in this work's calculations. The calculations were done using the Gaussian software package, version 09 (revision D.01)<sup>[98]</sup> using the hybrid functional B3P86 and def2-TZVP basis set. Oligomers of two, four, eight, and 12 units of EDOT were considered to show the shift of the thiophene ring deformation mode (shown in Figure 4d-i) with respect to oligomer size, as shown in Supporting Information Figure S10, granted that this system was usually observed in chains ranging from 5 to 20 units.<sup>[99,100]</sup> The obtained Raman frequencies were convoluted to a Lorentzian function of half-width at half-maximum of 2  $\text{cm}^{-1}$  for better visualization. Neutral and oxidized chains up to 33% and 50% (for the  $N = 12$ ) were considered to assess spectral signatures of polaronic and bipolaronic species.<sup>[101]</sup>

## Supporting Information

Supporting Information is available from the Wiley Online Library or from the author.

## Acknowledgements

The authors gratefully acknowledge Brazilian agencies (São Paulo Research Foundation FAPESP, Proc. Nos. 2015/26308-7; 2018/13492-2; and 2016/21070-5; the National Council for Scientific and Technological Development, CNPq (Grant 301553/2017-3); and Coordination of Improvement of Higher Level Personnel, CAPES) for their financial support. A.C.D.S. acknowledge FAPESP (Proc. Nos. 2014/09353-6 and 2017/00705-5) for scholarships granted, Dr. Igor O. Rocha (IQ-USP) for the discussions over the keratinocytes cell culture and Professor Leandro H. Andrade (IQ-USP) for the discussions over the degradation essays. V.H.P. acknowledge FAPESP (Proc. 2019/00207-0) for the funding and Professor Mónica B. M. López (UFABC) for the discussions over the PCA analysis.

## Conflict of Interest

The authors declare no conflict of interest.

## Author Contributions

A.C.D.S. and S.I.C.D.T. conceived the idea. A.C.D.S. planned and executed synthesis and electrochemistry experiments. A.C.D.S. and V.H.P. planned and executed spectroscopy experiments and quantum chemical calculations. I.O.R. assisted with keratinocytes cell culture. L.H.A., M.C.C.R., and S.I.C.D.T. discussed and analyzed all results. A.C.D.S. wrote the manuscript with input from all co-authors.

## Data Availability Statement

The data that support the findings of this study are available in the Supporting Information of this article.

## Keywords

biodegradable polymers, biomaterials, conducting polymers, graft-copolymers

Received: August 1, 2022  
Published online:

- [1] I. R. Minev, P. Musienko, A. Hirsch, Q. Barraud, N. Wenger, E. M. Moraud, J. Gandar, M. Capogrosso, T. Milekovic, L. Asboth, R. F. Torres, N. Vachicouras, Q. Liu, N. Pavlova, S. Duis, A. Larmagnac, J. Voros, S. Micera, Z. Suo, G. Courtine, S. P. Lacour, *Science* **2015**, 347, 159.
- [2] D. Afanasenkau, D. Kalinina, V. Lyakhovetskii, C. Tondera, O. Gorsky, S. Moosavi, N. Pavlova, N. Merkulyeva, A. V. Kalueff, I. R. Minev, P. Musienko, *Nat. Biomed. Eng.* **2020**, 4, 1010.
- [3] N. Wenger, E. M. Moraud, J. Gandar, P. Musienko, M. Capogrosso, L. Baud, C. G. Le Goff, Q. Barraud, N. Pavlova, N. Dominici, I. R. Minev, L. Asboth, A. Hirsch, S. Duis, J. Kreider, A. Mortera, O. Haverbeck, S. Kraus, F. Schmitz, J. Digiovanna, R. Van Den Brand, J. Bloch, P. Detemple, S. P. Lacour, E. Bézard, S. Micera, G. Courtine, *Nat. Med.* **2016**, 22, 138.
- [4] D. J. Chew, L. Zhu, E. Delivopoulos, I. R. Minev, K. M. Musick, C. A. Mosse, M. Craggs, N. Donaldson, S. P. Lacour, S. B. McMahon, J. W. Fawcett, *Sci. Transl. Med.* **2013**, 5, 210ra155.
- [5] C. Tondera, T. F. Akbar, A. K. Thomas, W. Lin, C. Werner, V. Busskamp, Y. Zhang, I. R. Minev, *Small* **2019**, 15, 1901406.
- [6] Y. Xu, P. A. Patsis, S. Hauser, D. Voigt, R. Rothe, M. Günther, M. Cui, X. Yang, R. Wieduwild, K. Eckert, C. Neinhuis, T. F. Akbar, I. R. Minev, J. Pietzsch, Y. Zhang, *Adv. Sci.* **2019**, 6, 1802077.
- [7] A. C. Da Silva, S. I. Córdoba De Torresi, *Front. Mater.* **2019**, 6, 98.
- [8] S. Alkan, L. Toppare, Y. Hepuzer, Y. Yagci, *J. Polym. Sci., Part A: Polym. Chem.* **1999**, 37, 4218.
- [9] R. Sarvari, S. Agbolaghi, Y. Beygi-Khosrowshahi, B. Massoumi, A. Bahadori, *J. Ultrafine Grained Nanostruct. Mater.* **2018**, 51, 101.
- [10] R. Sarvari, M. Akbari-Alanjaraghi, B. Massoumi, Y. Beygi-Khosrowshahi, S. Agbolaghi, *New J. Chem.* **2017**, 41, 6371.
- [11] A. Prasopthum, Z. Deng, I. M. Khan, Z. Yin, B. Guo, J. Yang, *Biomater. Sci.* **2020**, 8, 4287.
- [12] M. Xie, L. Wang, J. Ge, B. Guo, P. X. Ma, *ACS Appl. Mater. Interfaces* **2015**, 7, 6772.
- [13] C. Ding, Y. Wang, S. Zhang, *Eur. Polym. J.* **2007**, 43, 4244.
- [14] L. Huang, J. Hu, L. Lang, X. Wang, P. Zhang, X. Jing, X. Wang, X. Chen, P. I. Lekes, A. G. Macdiarmid, *Biomaterials* **2007**, 28, 1741.
- [15] B. Guo, A. Finne-Wistrand, A.-C. Albertsson, *Macromolecules* **2010**, 43, 4472.
- [16] L. Huang, X. Zhuang, J. Hu, L. Lang, P. Zhang, Y. Wang, X. Chen, Y. Wei, X. Jing, *Biomacromolecules* **2008**, 9, 850.
- [17] B. Guo, A. Finne-Wistrand, A.-C. Albertsson, *J. Polym. Sci., Part A: Polym. Chem.* **2011**, 49, 2097.
- [18] B. Guo, A. Finne-Wistrand, A.-C. Albertsson, *Biomacromolecules* **2010**, 11, 855.
- [19] J. Qu, Y. Liang, M. Shi, B. Guo, Y. Gao, Z. Yin, *Int. J. Biol. Macromol.* **2019**, 140, 255.
- [20] A. G. Guex, C. D. Spicer, A. Armgarth, A. Gelmi, E. J. Humphrey, C. M. Terracciano, S. E. Harding, M. M. Stevens, *MRS Commun.* **2017**, 7, 375.
- [21] A. J. Dominis, G. M. Spinks, L. A. P. Kane-Maguire, G. G. Wallace, *Synth. Met.* **2002**, 129, 165.
- [22] M. M. Ayad, N. A. Salahuddin, M. O. Alghaysh, R. M. Issa, *Curr. Appl. Phys.* **2010**, 10, 235.
- [23] V. Kumar, Y. Zhou, G. Shambharkar, V. Kunc, T. Yokozeki, *Synth. Met.* **2019**, 249, 81.

- [24] M. Cabuk, Y. Alan, M. Yavuz, H. I. Unal, *Appl. Surf. Sci.* **2014**, *318*, 168.
- [25] Y. Liang, B. Chen, M. Li, J. He, Z. Yin, B. Guo, *Biomacromolecules* **2020**, *21*, 1841.
- [26] C.-S. Wu, *Polym. Int.* **2012**, *61*, 1556.
- [27] E. Nazarzadeh Zare, M. Mansour Lakouraj, M. Mohseni, *Synth. Met.* **2014**, *187*, 9.
- [28] A. B. Abou Hammad, M. E. Abd El-Aziz, M. S. Hasanin, S. Kamel, *Carbohydr. Polym.* **2019**, *216*, 54.
- [29] Y. Li, N. Li, J. Ge, Y. Xue, W. Niu, M. Chen, Y. Du, P. X. Ma, B. Lei, *Biomaterials* **2019**, *201*, 68.
- [30] B. S. Kaith, R. Sharma, S. Kalia, *Int. J. Biol. Macromol.* **2015**, *75*, 266.
- [31] E. N. Zare, P. Makvandi, B. Ashtari, F. Rossi, A. Motahari, G. Perale, *J. Med. Chem.* **2020**, *63*, 1.
- [32] N. Baheiraei, H. Yeganeh, J. Ai, R. Gharibi, M. Azami, F. Faghihi, *Mater. Sci. Eng., C* **2014**, *44*, 24.
- [33] A. S. Widge, M. Jeffries-El, X. Cui, C. F. Lagenaur, Y. Matsuoka, *Biosens. Bioelectron.* **2007**, *22*, 1723.
- [34] H. He, L. Zhang, X. Guan, H. Cheng, X. Liu, S. Yu, J. Wei, J. Ouyang, *ACS Appl. Mater. Interfaces* **2019**, *11*, 26185.
- [35] L. Jin, T. Wang, Z.-Q. Feng, M. K. Leach, J. Wu, S. Mo, Q. Jiang, *J. Mater. Chem. B* **2013**, *1*, 1818.
- [36] M. Solazzo, K. Krukiewicz, A. Zhussupbekova, K. Fleischer, M. J. Biggs, M. G. Monaghan, *J. Mater. Chem. B* **2019**, *7*, 4811.
- [37] S. Střifteský, A. Marková, J. Vítěček, E. Šafaříková, M. Hrabal, L. Kubáč, L. Kubala, M. Weiter, M. Vala, *J. Biomed. Mater. Res., Part A* **2018**, *106*, 1121.
- [38] A. Madhan Kumar, A. Y. Adesina, M. A. Hussein, S. Ramakrishna, N. Al-Aqeeli, S. Akhtar, S. Saravanan, *Mater. Sci. Eng., C* **2019**, *98*, 482.
- [39] Y. Wu, L. Wang, B. Guo, P. X. Ma, *ACS Nano* **2017**, *11*, 5646.
- [40] R. Dong, P. X. Ma, B. Guo, *Biomaterials* **2020**, *229*, 119584.
- [41] X. Chen, Y. Wu, V. D. Ranjan, Y. Zhang, *Carbon* **2018**, *134*, 174.
- [42] K. Vallée-Rehel, V. Langlois, P. Guérin, A. Le Borgne, *J. Environ. Polym. Degrad.* **1999**, *7*, 27.
- [43] A. N. Zelikin, D. M. Lynn, J. Farhadi, I. Martin, V. Shastri, R. Langer, *Angew. Chem., Int. Ed.* **2002**, *41*, 141.
- [44] Y. Yagci, L. Toppare, *Polym. Int.* **2003**, *52*, 1573.
- [45] N. Kizilyar, U. Akbulut, L. Toppare, M. Y. Özden, Y. Yağci, *Synth. Met.* **1999**, *104*, 45.
- [46] A. Cirpan, S. Alkan, L. Toppare, G. David, Y. Yagci, *Eur. Polym. J.* **2001**, *37*, 2225.
- [47] A. Gürsel, S. Alkan, L. Toppare, Y. Yağci, *React. Funct. Polym.* **2003**, *57*, 57.
- [48] D. Mawad, K. Gilmore, P. Molino, K. Wagner, P. Wagner, D. L. Officer, G. G. Wallace, *J. Mater. Chem.* **2011**, *21*, 5555.
- [49] A. Domagala, W. Domagala, P. Ledwon, M. Musiol, H. Janeczek, A. Stolarczyk, P. Kurcok, G. Adamus, M. Lapkowski, *Polym. Int.* **2016**, *65*, 1395.
- [50] A. Türkan, F. Yılmaz, A. Ç. Küçük, Y. Özdemir, *Polym. Bull.* **2011**, *67*, 1483.
- [51] R. Mohammad-Rezaei, B. Massoumi, M. Abbasian, M. Eskandani, M. Jaymand, *J. Mater. Sci.: Mater. Electron.* **2019**, *30*, 2821.
- [52] B. Massoumi, M. Hatamzadeh, N. Firouzi, M. Jaymand, *Mater. Sci. Eng., C* **2019**, *98*, 300.
- [53] B. Massoumi, M. Abbasian, B. Khalilzadeh, R. Jahanban-Esfahlan, H. Samadian, H. Derakhshankhah, M. Jaymand, *Fibers Polym.* **2021**, *22*, 49.
- [54] B. Massoumi, M. Abbasian, B. Khalilzadeh, R. Jahanban-Esfahlan, A. Rezaei, H. Samadian, H. Derakhshankhah, M. Jaymand, *Int. J. Polym. Mater. Polym. Biomater.* **2020**, *70*, 693.
- [55] R. Sarvari, B. Massoumi, A. Zareh, Y. Beygi-Khosrowshahi, S. Agbolaghi, *Polym. Bull.* **2020**, *77*, 1829.
- [56] B. Massoumi, M. Abbasian, R. Jahanban-Esfahlan, R. Mohammad-Rezaei, B. Khalilzadeh, H. Samadian, A. Rezaei, H. Derakhshankhah, M. Jaymand, *Int. J. Biol. Macromol.* **2020**, *147*, 1174.
- [57] B. Massoumi, N. Sorkhishams, R. Sarvari, S. Agbolaghi, *Polym. Bull.* **2020**, *77*, 3707.
- [58] Y. S. Jeong, W.-K. Oh, S. Kim, J. Jang, *Biomaterials* **2011**, *32*, 7217.
- [59] A. C. Da Silva, T. Augusto, L. H. Andrade, S. I. Córdoba de Torresi, *Mater. Sci. Eng., C* **2018**, *83*, 35.
- [60] A. C. Da Silva, A. T. S. Semeano, A. H. B. Dourado, H. Ulrich, S. I. Córdoba De Torresi, *ACS Omega* **2018**, *3*, 5593.
- [61] M. Shen, T. A. Horbett, *J. Biomed. Mater. Res.* **2001**, *57*, 336.
- [62] A. Dominguez-Alfaro, E. Gabirondo, N. Alegret, C. M. De León-Almazán, R. Hernandez, A. Vallejo-Illarramendi, M. Prato, D. Mecerreyes, *Macromol. Rapid Commun.* **2021**, *42*, 2100100.
- [63] A. Dominguez-Alfaro, M. Criado-Gonzalez, E. Gabirondo, H. Lasa-Fernández, J. L. Olmedo-Martínez, N. Casado, N. Alegret, A. J. Müller, H. Sardon, A. Vallejo-Illarramendi, D. Mecerreyes, *Polym. Chem.* **2022**, *13*, 109.
- [64] A. Cho, S. Kim, S. Kim, W. Cho, C. Park, F. S. Kim, J. H. Kim, *J. Polym. Sci., Part B: Polym. Phys.* **2016**, *54*, 1530.
- [65] T. D. Y. Kozai, K. Catt, Z. Du, K. Na, O. Srivannavit, R. - M. Haque, J. Seymour, K. D. Wise, E. Yoon, X. T. Cui, *IEEE Trans. Biomed. Eng.* **2016**, *63*, 111.
- [66] U. Kraft, F. Molina-Lopez, D. Son, Z. Bao, B. Murmann, *Adv. Electron. Mater.* **2020**, *6*, 1900681.
- [67] D. J. Lipomi, J. A. Lee, M. Vosgueritchian, B. C.-K. Tee, J. A. Bolander, Z. Bao, *Chem. Mater.* **2012**, *24*, 373.
- [68] N. Kim, S. Lienemann, I. Petsagkourakis, D. Alemu Mengistie, S. Kee, T. Ederth, V. Gueskine, P. Leclère, R. Lazzaroni, X. Crispin, K. Tybrandt, *Nat. Commun.* **2020**, *11*, 1424.
- [69] X. Xin, Z. Xue, N. Gao, J. Yu, H. Liu, W. Zhang, J. Xu, S. Chen, *Synth. Met.* **2020**, *268*, 116503.
- [70] R. A. Green, R. T. Hassarati, L. Bouchinet, C. S. Lee, G. L. M. Cheong, J. F. Yu, C. W. Dodds, G. J. Suaning, L. A. Poole-Warren, N. H. Lovell, *Biomaterials* **2012**, *33*, 5875.
- [71] D. Mawad, C. Mansfield, A. Lauto, F. Perbellini, G. W. Nelson, J. Tonkin, S. O. Bello, D. J. Carrad, A. P. Micolich, M. M. Mahat, J. Furman, D. Payne, A. R. Lyon, J. J. Gooding, S. E. Harding, C. M. Terracciano, M. M. Stevens, *Sci. Adv.* **2016**, *2*, e1601007.
- [72] H. Shi, C. Liu, Q. Jiang, J. Xu, *Adv. Electron. Mater.* **2015**, *1*, 1500017.
- [73] K. Fukushima, C. Abbate, D. Tabuani, M. Gennari, G. Camino, *Polym. Degrad. Stab.* **2009**, *94*, 1646.
- [74] M. P. Arrieta, F. Parres, J. López, A. Jiménez, *J. Anal. Appl. Pyrolysis* **2013**, *101*, 150.
- [75] M. A. Elsayy, K.-H. Kim, J.-W. Park, A. Deep, *Renewable Sustainable Energy Rev.* **2017**, *79*, 1346.
- [76] A. C. Da Silva, M. J. Higgins, S. I. Córdoba de Torresi, *Mater. Sci. Eng., C* **2019**, *99*, 468.
- [77] M. N. Shkunov, W. Gellermann, Z. V. Vardeny, *Appl. Phys. Lett.* **1998**, *73*, 2878.
- [78] P. Almeida, C. Izumi, H. Santos, A. C. Sant'Ana, *Quim. Nova* **2019**, *42*, 1098.
- [79] J. E. P. da Silva, M. L. A. Temperini, S. I. C. de Torresi, *J. Braz. Chem. Soc.* **2005**, *16*, 322.
- [80] S. Garreau, G. Louarn, J. P. Buisson, G. Froyer, S. Lefrant, *Macromolecules* **1999**, *32*, 6807.
- [81] B. Guo, A. Finne-Wistrand, A. - C. Albertsson, *Macromolecules* **2012**, *45*, 652.
- [82] L. Li, M. Yu, P. X. Ma, B. Guo, *J. Mater. Chem. B* **2016**, *4*, 471.
- [83] R. Dong, X. Zhao, B. Guo, P. X. Ma, *ACS Appl. Mater. Interfaces* **2016**, *8*, 17138.
- [84] Y. Wu, L. Wang, B. Guo, P. X. Ma, *ACS Nano* **2017**, *11*, 5646.

- [85] Y. Liang, X. Zhao, T. Hu, B. Chen, Z. Yin, P. X. Ma, B. Guo, *Small* **2019**, *15*, 1900046.
- [86] J. Qu, X. Zhao, P. X. Ma, B. Guo, *Acta Biomater.* **2018**, *72*, 55.
- [87] A. C. Da Silva, R. A. Da Silva, M. J. P. G. Souza, P. M. Montoya, R. Bentini, T. Augusto, R. M. Torresi, L. H. Catalani, S. I. Córdoba de Torresi, *Biointerphases* **2020**, *15*, 021003.
- [88] R. A. Da Silva, R. Xue, S. I. C. De Torresi, S. Cartmell, *Biointerphases* **2022**, *17*, 011001.
- [89] S. Lindsay, *Life* **2020**, *10*, 72.
- [90] T. Q. Ha, I. J. Planje, J. R. G. White, A. C. Aragonès, I. Díez-Pérez, *Curr. Opin. Electrochem.* **2021**, *28*, 100734.
- [91] B. Zhang, E. Ryan, X. Wang, S. Lindsay, *J. Am. Chem. Soc.* **2021**, *143*, 15139.
- [92] J. Liu, Y. S. Kim, C. E. Richardson, A. Tom, C. Ramakrishnan, F. Birey, T. Katsumata, S. Chen, C. Wang, X. Wang, L.-M. Joubert, Y. Jiang, H. Wang, L. E. Fenno, J. B.-H. Tok, S. P. Paşca, K. Shen, Z. Bao, K. Deisseroth, *Science* **2020**, *367*, 1372.
- [93] A. da Silva, M. Minadeo, S. de Torresi, *J. Braz. Chem. Soc.* **2019**, *30*, 2066.
- [94] A. Allagui, T. J. Freeborn, A. S. Elwakil, B. J. Maundy, *Sci. Rep.* **2016**, *6*, 38568.
- [95] V. R. Feig, H. Tran, M. Lee, Z. Bao, *Nat. Commun.* **2018**, *9*, 2740.
- [96] H. Yuk, B. Lu, S. Lin, K. Qu, J. Xu, J. Luo, X. Zhao, *Nat. Commun.* **2020**, *11*, 1604.
- [97] G. Kister, G. Cassanas, M. Vert, *Polymer* **1998**, *39*, 267.
- [98] M. J. Frisch, G. W. Trucks, H. B. Schlegel, G. E. Scuseria, M. A. Robb, J. R. Cheeseman, G. Scalmani, V. Barone, B. Mennucci, G. A. Petersson, H. Nakatsuji, M. Caricato, X. Li, H. P. Hratchian, A. F. Izmaylov, J. Bloino, G. Zheng, J. L. Sonnenberg, M. Hada, M. Ehara, K. Toyota, R. Fukuda, J. Hasegawa, M. Ishida, T. Nakajima, Y. Honda, O. Kitao, H. Nakai, T. Vreven, J. A. Montgomery Jr., et al., *Gaussian 09*. **2009**.
- [99] D. Kim, I. Zozoulenko, *J. Phys. Chem. B* **2019**, *123*, 5160.
- [100] A. Ugur, F. Katmis, M. Li, L. Wu, Y. Zhu, K. K. Varanasi, K. K. Gleason, *Adv. Mater.* **2015**, *27*, 4604.
- [101] I. Zozoulenko, A. Singh, S. K. Singh, V. Gueskine, X. Crispin, M. Berggren, *ACS Appl. Polym. Mater.* **2019**, *1*, 83.